Models of bipolar charge transport in polyethylene

F. Boufayed, G. Teyssèdre,[a] and C. Laurent
Laboratoire de Génie Electrique, Toulouse III University and CNRS, Toulouse 31062, France

S. Le Roy and L. A. Dissado
Department of Engineering, University of Leicester, Leicester LE1 7RH, United Kingdom

P. Ségur
Centre de Physique des Plasmas et de leurs Applications, Toulouse III University and CNRS, Toulouse 31062, France

G. C. Montanari
Department of Electrical Engineering, University of Bologna, 41026 Bologna, Italy

(Received 20 January 2006; accepted 25 August 2006; published online 20 November 2006)

We introduce and develop two bipolar transport models which are based on appreciably different physical assumptions regarding the distribution function in the energy levels of trap states. In the first model, conduction is described by an effective mobility of the carriers and the accumulation of stored space charge is taken into account through a single trapping level. In the second model the hypothesis of an exponential distribution function of trap depth is made, with conduction taking place via a hopping process from site to site. The results of simulations of the two models are compared with experimental data for the external current and the space-time evolution of the electrical space charge distribution. The two descriptions are evaluated in a critical way, and the prospects for these models to adequately describe real systems are given. © *2006 American Institute of Physics*. [DOI: 10.1063/1.2375010]

I. INTRODUCTION

The use of polymeric materials, especially polyethylene as the insulation for high voltage (HV) cables, has grown steadily since they were introduced more than 30 years ago. Today polyethylene is rapidly becoming the preferred insulation material for even the highest transmission voltages. In respect to traditional oil-impregnated paper insulation, polyethylene exhibits quite beneficial characteristics, these being high reliability, low dielectric losses, and low environmental impact. However, under certain conditions, polyethylene may suffer from chemical, physical, and electrical aging or degradation after long-standing operation under voltage.[1] The degradation of the polyethylene may lead to electrical breakdown in the insulation of an alternating current (ac) or direct current (dc) cable. All of these factors when combined over time make the prediction of the probable working life of extruded cable very difficult. A problem for applications in high voltage dc (HVDC) transport is the propensity for polymeric insulation to accumulate charge through either injection at the interfaces or internal generation processes. These so-called space charges may produce field distortion within the insulation, and also catastrophic damage during the transmission of electrical energy. An understanding of space charge accumulation and its link to dielectric breakdown would be a major scientific achievement as well as facilitating the prediction of cable lifetime and the design of better cables. Nevertheless, the space charge accumulation and the related trapping-detrapping phenomena are still poorly understood. Over recent decades, a great deal of effort has been expended in developing experimental tools for space charge characterization,[2–6] in measuring space charges profiles,[7–9] or in identifying the different kinds of charges.[10,11] Meanwhile, only a few attempts have been made to provide some model description of these experimental results.[12–16]

We have initiated an activity which aims at modeling charge transport phenomena in a synthetic insulator largely used in the high voltage area: polyethylene. The aims are to account for the internal distribution of field as a function of stress, which could be used in the future to feed aging models, since, whatever the aging scenario considered, the local field is an important parameter. The transport model must be able to account for the distribution of electric charges (and of electric field) in nonstationary situations. The approach must be general enough to be applicable to a wide variety of insulators.

The aim of the present contribution is to compare two bipolar transport models that we have developed recently. The two models have been designed with the same objective, being to simulate charge transport in nonstationary conditions, but they are based on appreciably different physical assumptions regarding the distribution function in trap levels. For both models, carriers are provided only by charge injection at the electrodes. In the first model, conduction is described by an effective mobility of carriers, whereas for charge storage processes, space charge is taken into account through trapping in deep traps at a single specific energy level. In the second model, one makes the hypothesis of an exponential distribution function of trap depth, with conduction occurring via a thermally driven hopping process from site to site. The results produced by simulation of the two

[a]Electronic mail: gilbert.teyssedre@lget.ups-tlse.fr

models are compared with experimental data for the external current and the space-time evolution of the electric charge distribution.

II. MODEL DESCRIPTION

A. Common features

Even when neglecting dipolar processes and diffusion one generally has to solve the following coupled equations considering a one-dimensional (1D) problem along the spatial coordinate x, whatever the model used to describe charge transport:

for transport equation,

$$\frac{j(x,t)}{q} = \mu E(x,t) n(x,t), \tag{1}$$

for Poisson's equation,

$$\frac{\partial E(x,t)}{\partial x} = \frac{\rho(x,t)}{\varepsilon}, \tag{2}$$

for continuity equation,

$$\frac{\partial n(x,t)}{\partial t} + \frac{1}{q}\frac{\partial j(x,t)}{\partial x} = s(x,t), \tag{3}$$

where j is the transport current associated with each kind of carrier of density n and charge q, μ is the mobility, D is the diffusion coefficient, E is the applied field, and ρ is the net density of charge. Equations (1) and (2) are written for each kind of carrier defined in the model. The term s is the source term, i.e., it encompasses changes in local density due to processes other than transport, such as the internal generation of charges, recombination, etc. These equations have a specific form for the interfaces and are complemented by boundary conditions (e.g., applied voltage, etc.).

In the models, we have supposed that charge generation results from injection at the electrodes according to a Schottky law, being for electrons and holes,

$$j_e(0,t) = AT^2 \exp\left(-\frac{ew_{\mathrm{ei}}}{k_B T}\right)\exp\left[\frac{e}{k_B T}\sqrt{\frac{eE(0,t)}{4\pi\varepsilon}}\right], \tag{4}$$

$$j_h(D,t) = AT^2 \exp\left(-\frac{ew_{\mathrm{hi}}}{k_B T}\right)\exp\left[\frac{e}{k_B T}\sqrt{\frac{eE(D,t)}{4\pi\varepsilon}}\right], \tag{5}$$

where $j_e(0,t)$ and $j_h(D,t)$ are the fluxes of electrons and holes at cathode and anode, respectively, T is the temperature, $A = 1.2\times 10^6$ $\mathrm{Am^{-2}\,K^{-2}}$ is the Richardson constant, D is the interelectrode spacing, and w_{ei} and w_{hi} are the injection barriers for electrons and holes.

There is no extraction barrier, the extraction fluxes being $j_e(D,t)$ and $j_h(0,t)$ for electrons and holes at anode and cathode, respectively;

$$j_{e,h}(z,t) = \mu_{e,h} E(z,t) \rho_{f(e,h)}(z,t). \tag{6}$$

The total current density, $J(t)$ is obtained from second Maxwell's equation, that is

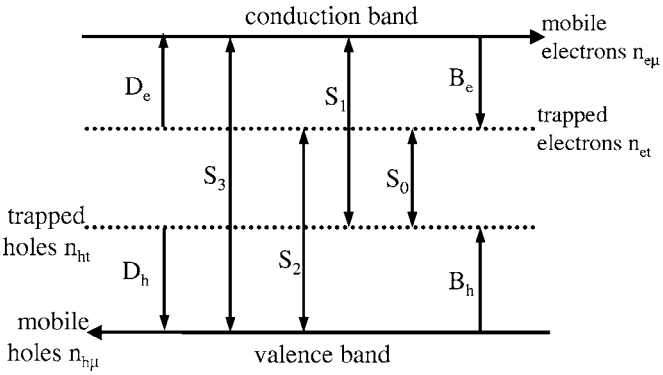

FIG. 1. Schematic representation of the conduction and trapping coefficients for model I. S_i are recombination coefficients, $n_{e\mu}$, n_{et}, n_{ht}, $n_{h\mu}$ are mobile and trapped electron and hole densities, and B_i and D_i are trapping and de-trapping coefficients.

$$J(t) = j(x,t) + \varepsilon\frac{\partial E(x,t)}{\partial t}. \tag{7}$$

The first term of the right-hand side is the conduction contribution and the second term is the displacement current. It can be shown that Eq. (7) can be rewritten as

$$J(t) = -\frac{\varepsilon}{D}\frac{dV(t)}{dt} + \frac{1}{D}\int_0^D j(x,t)dx. \tag{8}$$

Note that dV/dt is null in the present simulation conditions.

B. Model I

Model I, which has already been described in several papers,[12,17,18] is depicted in Fig. 1. Two kinds of carriers are considered, being either trapped or mobile. A mobile electron in the conduction band (hole in the valence band) is associated with an effective mobility. This mobility accounts for the possible trapping and detrapping in shallow traps, in which the time of residence is short ($\approx 10^{-12}$ s).[12,19,20] Deep trapping (coefficients B_i) is described through a single trapping level for each kind of carrier. Charge carriers have a certain probability to escape from deep traps by overcoming a potential barrier that is included in the detrapping coefficients D_i. The recombination of carriers is accounted for considering different coefficients S_i for the several electron-hole pairs. After recombination, the trap is released and trapping, thus becomes possible again. A small quantity of mobile negative and positive charges (up to 0.5 $\mathrm{C\,m^{-3}}$) is supposed to be initially distributed uniformly within the dielectric while keeping it electrically neutral (the local net charge density is null). Taking into account the nonpolar character of polyethylene, dipolar polarization has been neglected. Also, the internal generation of carriers is not considered. An example of an expression for the source term of Eq. (3) is given for mobile electrons in Eq. (9),

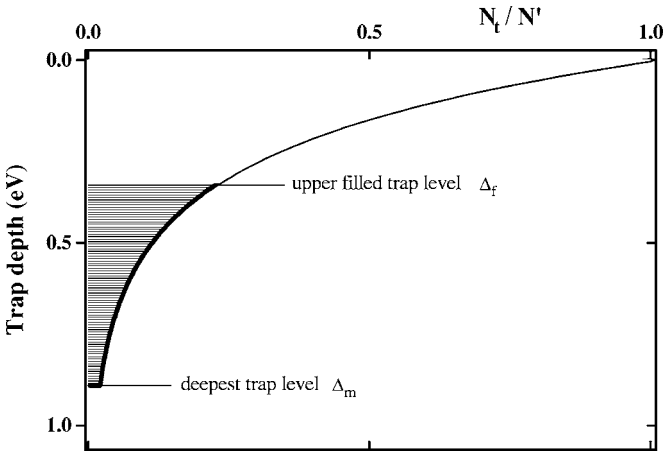

FIG. 2. Exponential distribution of trap levels for one kind of carriers. The upper filled level Δ_f is variable as a function of time and space.

$$s_1 = \frac{\partial n_{e\mu}}{\partial t} = -S_1 n_{\mathrm{ht}} n_{e\mu} - S_3 n_{h\mu} n_{e\mu} - B_e n_{e\mu}\left(1 - \frac{n_{\mathrm{et}}}{n_{0\mathrm{et}}}\right) + D_e n_{\mathrm{et}}, \tag{9}$$

where S_i are the recombination coefficients, B_e is the trapping coefficient for electrons, $n_{e\mu}$ and $n_{h\mu}$ are mobile electron and hole densities, n_{et} and n_{ht} are the densities of trapped electrons and holes, and $n_{0\mathrm{et}}$ and $n_{0\mathrm{ht}}$ are the trap densities for electrons and holes. Note that the source term is expressed here in terms of the carrier density whereas it is in charge density in earlier definitions.[12,17] The detrapping probability is defined by a detrapping coefficient, for each species, which is of the form

$$D = \nu \exp\left(\frac{-w}{k_B T}\right), \tag{10}$$

where ν is the attempt to escape frequency, which has been set to $k_B T/h = 6.2 \times 10^{12}\ \mathrm{s}^{-1}$ at room temperature, T is the temperature, and w is the detrapping barrier.

C. Model II

The main feature of model II is that an exponential distribution of trap depths is considered and that the same ensemble of carriers moves site to site and participates in deep trapping. For the sake of simplification, charge recombination has not been included in the model. With these two hypotheses, the source term in Eq. (3) is null in this case.

1. Trap distribution

The exponential distribution (Fig. 2) has been truncated by defining a maximum trap depth in order to avoid extremely low values of mobility at low charge density,

$$N_{t(e,h)}(\Delta_{e,h}) = N'_{e,h} \exp\left[-\frac{\Delta_{e,h}}{k_B T_{0(e,h)}}\right] \quad (\Delta \leqslant \Delta_m). \tag{11}$$

Here $N_{t(e)}$ and $N_{t(h)}$ (in $\mathrm{m}^{-3}\,\mathrm{J}^{-1}$) are the trap density distributions, respectively, for electrons and holes, characterized by a shape parameter T_0, the preexponential factor N', and maximum trap depth Δ_m.

2. Transport and trapping

Traps are supposed to be filled from the deepest levels upwards.[13] This means that an upper filled level, $\Delta_f\ (x,t)$, can be defined, which is time and space dependent. The relation between carrier density, for one specie, and Δ_f is of the form

$$n_{(e,h)} = \int_{\Delta_f}^{\Delta_m} N_{t(e,h)}(\Delta_{e,h})\, d\Delta, \tag{12}$$

which gives

$$\Delta_f = k_B T_0 \ln\left[\frac{n_{e,h}}{N' k_B T_0} + \exp\left(-\frac{\Delta_m}{k_B T_0}\right)\right]. \tag{13}$$

Charge transport within insulating polymers is often described by a hopping mechanism in which carriers move from site to site by getting over a potential barrier. In our case the hopping charges essentially come from the highest filled trap state at a depth Δ_f, and the resulting mobility has the form[13]

$$\mu(E) = \frac{2\upsilon d}{E} \exp\left(-\frac{\Delta_f}{k_B T}\right) \sinh\left(\frac{eEd}{2k_B T}\right), \tag{14}$$

where d is the average distance between traps and e is the elementary charge.

When $T \ll T_0$, only a fraction n_f of the total carrier density n is involved in transport: this corresponds effectively to carriers trapped at an energy within $k_B T$ in respect to Δ_f,[13,21,22]

$$n_f = \frac{n}{1+a} \quad \text{with } a = \frac{T_0}{T}. \tag{15}$$

The average intersite distance d is related to the trap density according to

$$d = (N' k_B T_0)^{-1/3} \left[1 - \exp\left(-\frac{\Delta_m}{k_B T_0}\right)\right]^{-1/3}. \tag{16}$$

Hence, once the shape parameters for the distribution function have been settled, the mobility is entirely defined regarding its temperature, field, and carrier density dependencies.

3. Model parameters

One way to proceed for parameterizing the distribution is to consider literature data on trap density estimates.[23] Quirke and co-workers[19,24,25] developed molecular simulation aimed at estimating the trap depth associated with given chemicals in polyethylene, along with those for physical traps associated with disorder in chain conformation. The results of these simulations for electronic carriers are shown in Fig. 3. In order to compare the continuous distribution used in model II and the discrete distribution obtained by molecular simulation, we have integrated the continuous distribution function on adjacent intervals of width of 0.2 eV between 0 and 1.2 eV, setting the distribution parameters to

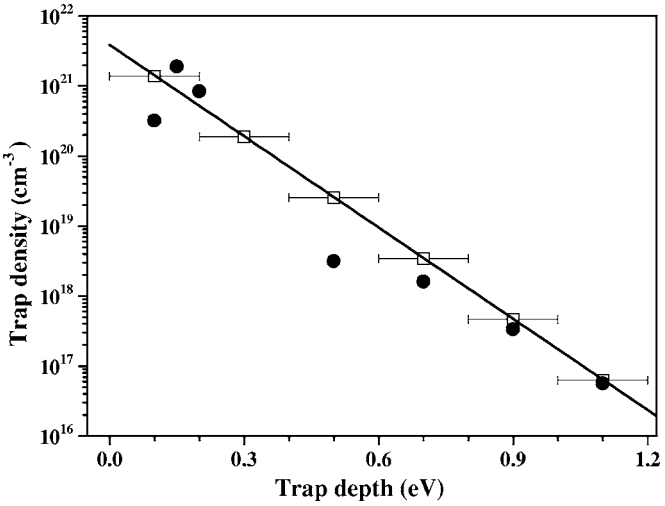

FIG. 3. Discrete distribution of electron trap density as a function of trapping energy. The circles are results of Quirke's molecular simulation of Meunier *et al.* (Ref. 24). The continuous distribution function used in model II (solid line with $N'=10^{47}$ m^{-3}J^{-1} and $T_0=1160$ K) has been integrated on adjacent intervals of width of 0.2 eV (squares).

$N'=10^{47}$ m^{-3} J^{-1} and $T_0=1160$ K. The exponential distribution reasonably accounts for these molecular simulation results. Actually, simulation data are available only for electron traps, and only a limited amount of chemicals has been considered in this work. In addition, these simulations were relevant to cross-linked polyethylene rather than low density polyethylene (LDPE). Nevertheless, this comparison shows that the hypothesis of an exponential distribution of traps can be realistic.

D. Resolution and application

The numeric techniques implemented to solve the set of equations are basically the same for the two models.[26] Briefly, the electric field and potential in the dielectric are calculated with a boundary element method (BEM).[27] With this method, the computation is more rigorous than by using discretization of Poisson's equation, and furthermore the field is known on every point in the dielectric, including the electrodes. Our numerical model employs a specific numerical method of solution of the continuity equation in order to accurately resolve the steep fronts that may appear in the electron and hole densities. This numerical method is based on a numerical scheme initially developed by Leonard[28] (quickest scheme) that we extended to very general situations. This scheme is employed with a specific flux limiter that guarantees that all particle densities are positive. The cell used for computation is divided into elements Δx, of varying length, being tightened close to the electrodes in order to optimize numeric computation. The time step in the computation is chosen automatically depending on the variation rate in the computed parameters. It must satisfy the condition of Courant-Friedrichs-Lewy,[29] (CFL) in a manner so as to guarantee the stability of the numerical scheme.

In respect to model I, model II may appear simpler, since only two ensembles of parameters are defined: that associated with carrier generation at the electrodes, being the same as for model I, and the set of quantities defining the shape of the trap-energy distribution. Since mobile and trapped species are not differentiated, there are only two kinds of species (instead of four). In addition, the source terms are null. Table I compares the main features of the two models.

TABLE I. Features of the models.

Features	Model I	Model II
General characteristics	Bipolar model	Bipolar model
Trap levels	One level of deep traps	Exponential distribution
Transport	Effective mobility	Hopping conduction
Transport vs trapping	Trapping coefficients Detrapping barriers	Fraction of trapped charge involved in transport
Charge generation	Schottky injection	Schottky injection
Charge extraction	No extraction barrier	No extraction barrier
Recombination	Recombination coefficients	Not accounted for

Model I has been applied successfully to simulate the time dependence of space charge density profiles, external current, and electroluminescence considering measurements realized in charging/discharging conditions, along with various protocols for dc stress applications.[18,30] Such work led to a set of parameters, reported in Table II that appears suitable to describe the behavior of LDPE. The first objective of this work is to compare the outputs of the two models for initial conditions that are as close as possible. In Sec. IV, the parametrization of model II is improved in respect to the experimental behavior.

III. COMPARISON OF MODEL OUPUTS

In this section, we attempt to parametrize model II as closely as possible to model I and we discuss the differences between the two approaches. As an experimental basis, we have considered the charging and discharging behaviors of a 150 μm thick LDPE film with 40 kV/mm applied field and 3 h of charging/discharging time at room temperature. Ex-

TABLE II. Sets of parameters used for comparing models I and II (sets II.1 and II.2) and to fit to experimental data (set II.3).

Model I		Model II			
Set	I.1	Set	II.1	II.2	II.3
B_e (s^{-1})	0.10	T_{0e} (K)	2.10^4	3.10^5	800
B_h (s^{-1})	0.20	T_{0h} (K)	2.10^4	3.10^5	860
w_e (eV)	0.96	N'_e (m^{-3} J^{-1})	10^{46}	10^{46}	9.10^{44}
w_h (eV)	0.99	N'_h (m^{-3} J^{-1})	10^{46}	10^{46}	5.10^{44}
$S_0=S_1=S_2$ (m^3 s^{-1})	$6.4\ 10^{-22}$	Δ_{me} (eV)	0.608	0.605	1.00
S_3 (m^3 s^{-1})	0	Δ_{mh} (eV)	0.534	0.532	0.83
$n_{0e}=n_{0h}$ (m^{-3})	$6.25\ 10^{20}$				
μ_e (m^2 V^{-1} s^{-1})	1.10^{-14}				
μ_h (m^2 V^{-1} s^{-1})	2.10^{-13}				
w_{ei} (eV)	1.27	w_{ei} (eV)	1.27	1.27	1.30
w_{hi} (eV)	1.16	w_{hi} (eV)	1.16	1.16	1.00
$\rho_h=\rho_e$ (C m^{-3}), $t=0$	0.5	$\rho_h=-\rho_e$ (C m^{-3}), $t=0$	0.5	0.5	0.5

perimental data on space charge measurements[18] have been obtained by the pulsed electroacoustic (PEA) technique.

The results produced by either model cannot be directly compared to experimental data, especially the space charge profiles obtained by the PEA method, firstly because only internal charges are produced by the simulation that do not influence charges on the electrodes; secondly, profiles obtained by the PEA method are, as with any other technique, accompanied by uncertainty in the position of the charges. As it is not possible in practice to correct experimental data for the uncertainty associated with charge position, we have applied a numerical filter to our data in order to lose part of the resolution reached by the simulated profiles.[31] The figures produced for the space charge evolution are maps of the net charge density inside the sample as a function of time. Each map has three dimensions: thickness (Y axis), time (X axis), and charge density, which is represented by a color scale. Space charge profiles are produced at time intervals that are shorter at the beginning of the polarization and depolarization phases in order to improve resolution. Hence, the time scale is not linear, but is the same for experiment and simulation.

We have considered that charges can be present initially in the material: the density for positive and negative charges is the same so that the net charge density, i.e., that probed by any space charge measurement method, is null. This hypothesis did lead to consistency between experimental and simulated electroluminescence transients at short time when using model I.[30]

A. Mobility versus field and charge density for model II

Whereas injection conditions could be taken as rigorously the same for the two models, the hypotheses used did not allow the same to be said of the mobility. A fixed mobility is set in model I whereas Eq. (14) shows that μ is dependent on charge density and field, and that the three parameters of the distribution control this dependency,

$$\mu(n,E) = \frac{2\upsilon d}{E}\exp\left(-\frac{\Delta_m}{k_BT}\right) \times\left[1+\frac{n}{N\prime\, k_BT_0}\exp\left(\frac{\Delta_m}{k_BT_0}\right)\right]^a \sinh\left(\frac{eEd}{2k_BT}\right). \tag{17}$$

Even when $n=0$ and $E=0$, the mobility is dependent on the three parameters and several combinations of N', Δ_m, and T_0 may give a preset mobility.

When $kT_0 \gg \Delta_m$, which is so for T_0 of the order of 10^3K and Δ_m of the order of 1 eV, the intertrap distance [Eq. (16)] can be approximated to $d=(N\prime\, k_BT_0)^{-1/3}$ so that at low carrier density, the parameters controlling $\mu(n,E)$ are N', T_0, and Δ_m. However, it can be readily observed that the variation of mobility with carrier density is stronger when T_0 is small. Therefore an approach to the conditions of a mobility independent from the charge density requires a relatively high T_0. The variation of mobility with field will be weaker as d becomes smaller, i.e., N', T_0 large to a first approximation. There is finally a constraint on the value of mobility: we have arbitrarily chosen a value of Δ_m such that $\mu(0,0)$ equals that used in model I.

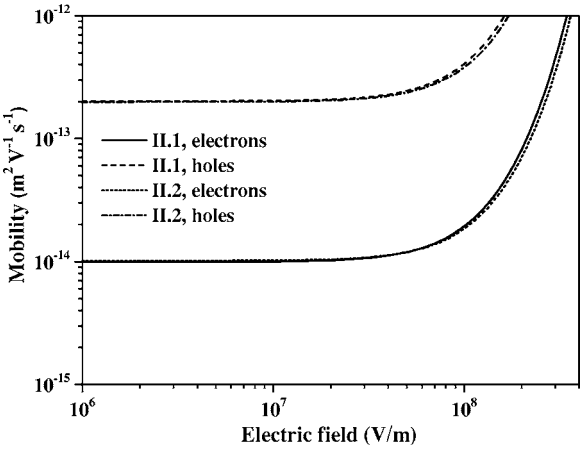

FIG. 4. Electron and hole mobilities vs field for model II. Two sets of parameters are considered (II.1 and II.2). The carrier density is set to $n_e = n_h = 0$. The mobility significantly increases at field in excess of 50 kV/mm.

Table II shows the combinations of parameters that have been tested (sets II.1 and II.2), and Fig. 4 shows how the mobility varies with field for both electrons and holes in these conditions. The mobility significantly increases at fields in excess of 50 kV/mm. It is independent of charge density up to at least 10^3 C/m^3.

B. Results

Figure 5 compares space charge patterns obtained using the two models for a 150 μm thick sample under 40 kV/mm dc stress at 293 K. The charging and discharging times were 3 h. In both cases, space charge profiles appear dominated by positive carriers, a feature which arises from the significantly lower Schottky barrier for holes (1.16 eV) as compared to electrons (1.27 eV). It can readily be seen that different results are obtained in the two models. The accumulated charge density appears lower in the case of model II. Charge release during depolarization can be more clearly seen in the case of model I. The transit time for the first positive charge front also changes, depending on the situation. It is about 20 s for set I.1, 1000 s for II.1, and beyond 3 h for II.2.

Figure 6 compares the charging current transients obtained in the two cases. Here again, quite different behaviors are predicted. Model I predicts a continuous decrease of the current, whereas in model II the current increases, forms a peak, decreases for a while, and then increases again. In model I, the current increased up to a maximum and then decreased when supposing that no initial charges were present.[12] Such shapes, especially the peak in current transient, are more generally characteristic of space-charge-limited current transients.[32] In our simulations, the initial current is higher when the initial charge density is large. Obtaining a decaying transient current is a matter of balance between charge injection and transport, a favorable situation being roughly strong injection associated with slow transit.

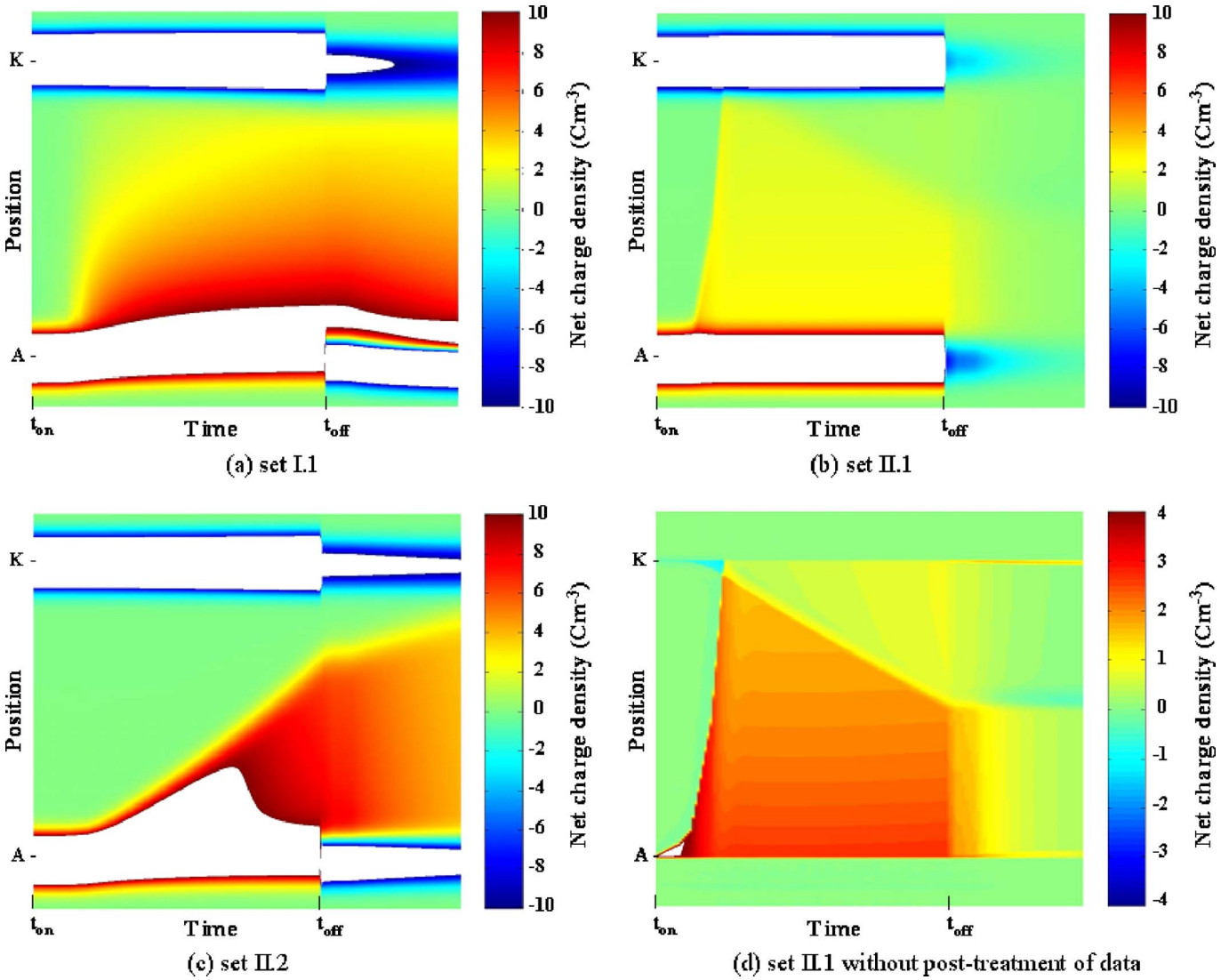

FIG. 5. (Color online) Net charge density vs time for a 3 h/3 h polarization/depolarization cycle simulated using parameters of Table II. t_{on} and t_{off} stand for the time of voltage application/short circuit. *A* and *K* stand for anode and cathode, respectively. The accumulated charge density is lower in the case of model II. The transit time for the positive charge front varies from (a) 20 s to (b) 1000 s (not clearly evidenced in the figures as commented in the discussion part) and to (c) 3 h.

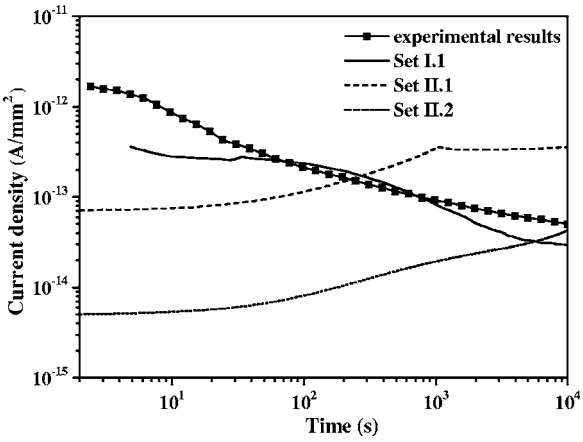

FIG. 6. Charging current transients produced by models I and II (with two sets of parameters) and obtained experimentally for a field of 40 kV/mm at 293 K. For model II, the current rises in time, being in contradiction to experimental features.

C. Discussion

Supposing that positive carriers are dominant and that there is not much field distortion within the insulation, the transit time for carriers being at the charge front should be governed by the group velocity of carriers defined by

$$w_G = \frac{n_{h\mu}}{n_h}\mu E_a, \tag{18}$$

where $n_{h\mu}$ and n_h are the density of mobile holes and the total density of holes, respectively, and E_a is the applied field. In the case of model II, the fraction of mobile carriers is readily obtained from Eq. (15). The expected transit times for sets II.1 and II.2 are 1250 and 18 750 s for a 150 μm thick sample. Inspection of charge profiles shows that the transit times are about 1000 s for set II.1 and about 13 500 s for set II.2, as deduced from simulation during long polarization time (30 000 s). These transit times exactly correspond to the peak in the charging current. The fact that the transit time obtained in simulation is slightly shorter than

expected comes mainly from field distortion due to space charge (the field at the charge front exceeds the applied field by up to 20% of the applied field), and possibly to some extent to the value of mobility which is slightly above 2×10^{-13} m^2 V^{-1} s^{-1} at 40 kV/mm. In the case of set II.2, it can be observed that the velocity of charges tends to increase once they have crossed about half of the insulation, and this behavior results from field distortion (up to 20% intensification). Hence, for the case II.1, positive charges move more freely in the insulation and less accumulation than in case II.2 is observed, since accumulation is a matter of balance between generation and transport. This mechanism is confirmed considering Fig. 6 where the external current is higher in case II.1.

For model I, the transit time for the injected charge front to reach the counterelectrode is much shorter, being about 20 s, even if this is not clearly evidenced in the figures, as commented in the following. In addition to transport, trapping, and detrapping, model I allows for recombination processes. The criticality study achieved on this aspect[33] showed that for recombination parameters in the range of 10^{-1}–10^{-5} m^3 C^{-1} s^{-1}, recombination processes contribute only marginally to the change in local density of carriers. Hence, recombination processes do not constitute the leading factor in the difference between the two models. Neither does the assumption of an initial density of charges since the space charge and current profiles are not influenced at times beyond 10 s, for $\rho_h = \rho_e(t=0)$ in the range of 0–0.5 C/m^3. As mobility is quasiconstant in either case, the differences between the two models in the charging behavior have to be found in the number of carriers available for conduction. In the case of model II, the fraction of charges involved in conduction [Eq. (15)] is of the orders of 1.5×10^{-2} and 10^{-3} for the set of parameters II.1 and II.2, respectively. For model I, the fraction of mobile positive charge with respect to the total amount of positive charge carriers is more difficult to estimate since it results from trapping, detrapping, and recombination probabilities and it is dependent on time and space. However, a simple analytical solution for the transit time of the charge front injected at time zero can be obtained under the approximations that internal field distortion due to space charge and trapped charge densities is negligible: only trapping is allowed for during transport. With these hypotheses, the transport equation for mobile holes can be rewritten as

$$\frac{\partial n_{h\mu}(x,t)}{\partial t} + w\frac{\partial n_{h\mu}(x,t)}{\partial x} = -B_h n_{h\mu}(x,t) \quad \text{with } w = \mu E_a. \tag{19}$$

Considering that $n_{h\mu}(x,t)=0$ for $t \leqslant 0$, the solution is of the form

$$n_{h\mu}(x,t) = n_{h\mu}(x - wt, 0)e^{-B_h t}. \tag{20}$$

Equation (20) shows that the injected front is attenuated during propagation and that no qualitative distortion of the charge front occurs during transport. From the parameter set I.1, the time necessary for the front to reach the counterelectrode ($x = wt = 150$ μm) is estimated to be 18.8 s, in good agreement with the simulation results. A strong attenuation of the mobile hole density is predicted (about 2.5% of the charges injected at time 0 reach the counterelectrode): this feature explains why in simulated profiles of Fig. 5(a) a time much longer than 20 s is necessary for observing an appreciable amount of positive carriers approaching the cathode. Even though there is an attenuation of mobile carrier density due to trapping, the fraction of mobile carriers remains much higher than for model II; as a consequence, the charging current is stronger in model I at short time.

Model I gives stronger charge accumulation and less current density than model II in the long term. The only explanation for this behavior is that as time goes on, the fraction of carriers involved in conduction becomes smaller, i.e., the proportion of trapped charges is continuously increasing. Carriers are assumed to be mobile immediately after being injected. They are progressively trapped during transport. As time goes on, fewer charges are injected due to the field decrease at the anode, and hence the proportion of trapped charges grows. Of course, other phenomena such as detrapping and recombination contribute to the balance between trapped and mobile carriers.

It can be seen in Fig 5(b) (model II) that the positive charge density decreases in the vicinity of the cathode at long times. This corresponds to injection of negative carriers. Figure 5(d) shows density profiles for the set of parameters II.1 using a different representation: post-treatment of data was not achieved and, in addition, the charge density color scale is different. The injection of negative carriers clearly appears in this picture. The increase in the charging current observed at long time scale (Fig. 6) corresponds to the response of the material when electron transport significantly contributes to the external current. Injected negative carriers progressively penetrate into the insulation, thus diminishing the net charge. Model I also predicts negative charge injection and drift in the bulk. Negative charges are the dominant carriers up to 20 μm from the cathode at the end of the polarization stage.

IV. APPROACH TO EXPERIMENTAL RESULTS FOR MODEL II

A. Distribution parameters

In the above attempt to compare the two models for a near identical parameter system, it appears that the predicted external transient current for model II does not have the same shape as the experimental behavior (Fig. 6). Also, the internal charge density appears less than the experimental one [the latter is shown in Fig. 7(a)]. Consequently a new set of parameters has been looked for in order to find an agreement with the experimental results.

As stated previously, in situations dominated by transport of one kind of carrier, the models predict that a decreasing charging current is obtained once the front of charges has reached the counterelectrode. However, the experimental current is continuously decreasing in the time range when data are available, whereas a front of positive carriers moves slowly in the space charge measurements. There could be other origins to the current at short time such as orientation polarization. Polyethylene is a weakly polar material, and

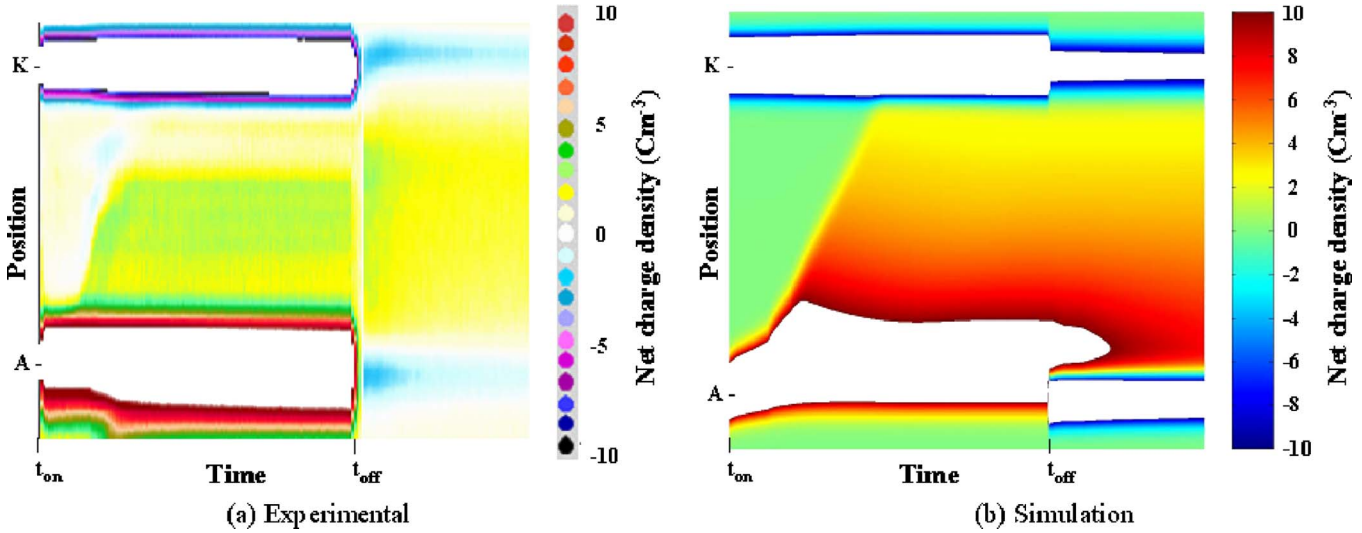

FIG. 7. (Color online) Experimental and simulated net charge densities vs time using the optimized parameters of set II.3. t_{on} and t_{off} stand for the time of voltage application/short circuit. *A* and *K* stand for anode and cathode, respectively. Note that the color scale is not the same due to different softwares for handling data. The simulated charge density is overestimated in the charging period and the discharging is slower than expected.

though this possibility cannot be completely discarded due to a lack of experimental data on the order of magnitude of polarization effects, we suppose for the moment that the response is dominated by transport.

Some simulation conditions break the above rule on the relation between charge front and transient current shape. First, if the response is dominated by the transport of preexisting carriers, then a decreasing charging current is obtained. Second, in situations where massive injection occurs associated with significant charge accumulation (strong field distortion), again the current becomes continuously decreasing. A way to favor injection in respect to transport is to decrease the barrier height to injection and/or to decrease the fraction of mobile carriers by decreasing T_0. The fit to the experimental behavior, especially as regards the transient current, has been improved by acting on these two factors. The final set of parameters is given in Table II, set II.3. As previously, the injection barrier for holes is significantly lower than that for electrons.

In the set of parameters II.3, T_0 is smaller than that (1160 K) estimated from the simulation data of Quirke and co-workers (cf. Fig. 3 for electron traps). In fact, the slope of the curve (in semilog coordinates) is governed mainly by the density of deep traps. As Quirke and co-workers have considered cross-linked polyethylene (XLPE) as a model material, they have incorporated cross-linking by-products as potential deep traps. Consequently, LDPE should contain a lower concentration of deep traps, and hence T_0 is expected to be smaller for LDPE. The preexponential factor N'_e is about 10^{45} m^{-3} J^{-1}, which is somewhat lower than that obtained by regression in Fig. 3 (10^{46}–10^{47} m^{-3} J^{-1}), indicating that not necessarily all physical traps are involved in transport. Overall, the distribution parameters obtained can be considered as physically conceivable.

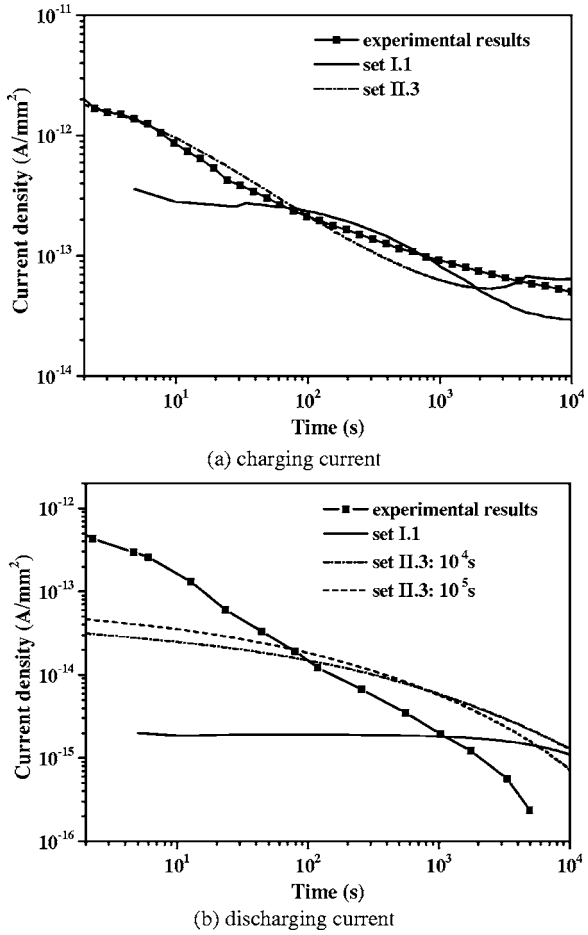

FIG. 8. Experimental charging and discharging current densities compared to results from models I and II (set II.3). The discharging currents correspond to previous polarization for 10^4 s for model I, for 10^4 and 10^5s for model II, and for 10^5 s in experiment. Whereas the charging current can be approximately fitted with either model, the discharging current decays more slowly than experimentally measured.

B. Results and discussion

With this set of parameters, the transient charging current (Fig. 8) is predicted both quantitatively and qualitatively,

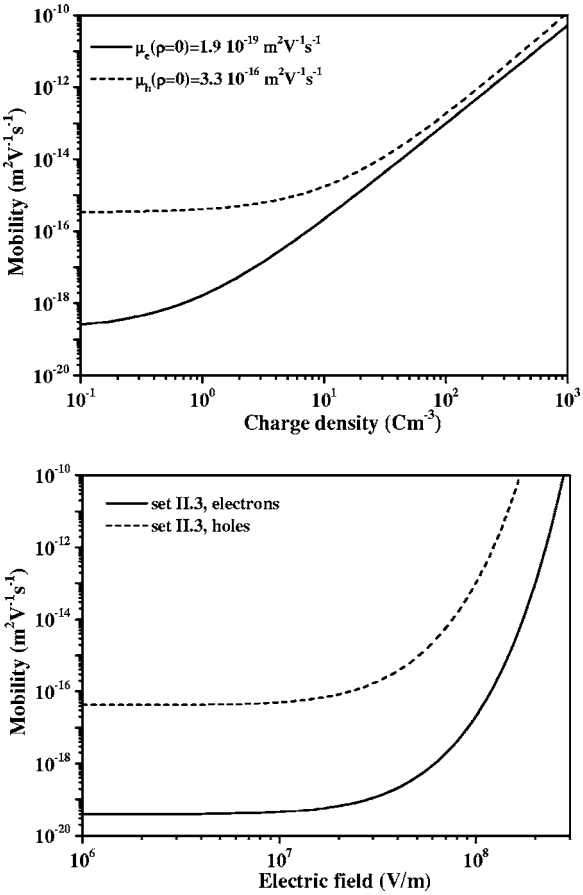

FIG. 9. Mobility as a function of charge density (for $E=40$ kV/mm) and field (for $\rho=0$) for parameter set II.3. The mobility is significantly dependent on both charge density and field, even at moderate values.

except at long charging times when possible transport of negative carriers comes into play. The charge density (Fig. 7) is overestimated in the charging period. In the discharging period, charges apparently move too slowly in respect to the experimental behavior. This feature was already noticed in model I. In respect to case studies II.1 and II.2, mobility becomes strongly dependent on field and charge density, as shown in Fig. 9. For a charge density of the order of 30 C/m^3, the mobility for $E=40$ kV/mm is of the same order as that of model I. However, for low charge densities (i.e., at short polarization time), the mobility is small (order of 10^{-16} m^2 V^{-1} s^{-1} for holes), thereby favoring accumulation in respect to trap-to-trap hopping transport.

Experimentally, it can be estimated that the front of positive charges reaches the counterelectrode within roughly 2500 s. The transit time for the front of positive carriers is 4000 s in simulation, which is somewhat higher than the experimental value and which is consistent with that deduced from Eq. (18) (4900 s), taking into account velocity enhancement due to field distortion at the charge front. Again, the time at which the positive charge front reaches the counterelectrode corresponds to the peak at 4000 s in the transient current (Fig. 8). It is worth pointing out here that simultaneous measurement of space charge and current at high field, i.e., in conditions where packetlike behavior was observed in XLPE, demonstrated that the external current is at a maximum at the time a packet reaches the counterelectrode.[34,35]

The anode field for set II.3 decreases very quickly from 300 s onwards, being of the order of 10^4 V/m. Hence, it is expected that the contribution from electron transport becomes significant at long times; it is, however, not necessarily so at 10^4 s since the negative charge extends up to only about 12 μm from the cathode, with a density not exceeding -5 C/m^3.

For low fields (as in the depolarization stage), the mobility is low. The minimum value for hole mobility is $\mu(0,0)=4\times10^{-17}$ m^2 V^{-1} s^{-1}. Discharging is observed anyway in space charge profiles since a relatively high charge density is present initially, and a large fraction (about 25%) of carriers is mobile. Figure 8(b) shows discharging currents obtained experimentally after 10^5 s of polarization. For model II, though orders of magnitude of the current could be reproduced in a certain time interval, the depolarization current decays more slowly than experimentally measured. This is most probably related to an underestimated mobility during depolarization. In the case of model I.1, the depolarization current is even lower. As stated above, in this model the fraction of trapped charges is continuously growing during the polarization stage so that a large majority of carriers stay in deep traps after 3 h of polarization. Hence, in this case, the detrapping probability has to be considered rather than the mobility as the rate limiting step in depolarization. Clearly, depolarization currents could not be reproduced satisfactorily by either model. There could be two reasons for this. Firstly, depolarization features are primarily dependent on the actual space charge distribution set up at the end of the polarization stage. Experimental data were obtained in independent experiments, the polarization time being longer for current (10^5 s) than for space charge profiles (10^4 s), so that we actually do not know what was the space charge profile prior to the depolarization current measurements. Simultaneous measurement of current and space charge could be advantageous in this respect since it would provide the actual space charge distribution built up prior to discharging current measurement. Secondly, as stated previously, attempting to reconcile experimental and simulated transient currents could be misleading, as other processes, such as orientation polarization, and possibly ionic contributions could contribute to the current without observable effects in space charge measurements.

V. CONCLUSION

Two bipolar transport models aimed at accounting for the space charge accumulation and transient current in LDPE under dc stress have been presented and compared. The first model considers mobile and trapped carriers as distinct species, a field-independent effective mobility being associated with the former and a single deep trapping level to the latter. Exchanges between the different kinds of species are governed by trapping, detrapping, and recombination probabilities. In the second model, an exponential distribution of trap levels is considered, the same ensemble of carriers being involved in trapping and transport. In this case, a thermally assisted hopping mobility is considered, being charge density and field dependent. Carriers are provided by Schottky injec-

tion in both cases. It is shown that the two models are not equivalent, regarding the kinetics of space charge buildup within the insulation and the transient currents. The proportion of trapped charges increases during the time under stress for model I, whereas it is constant in model II. As a consequence, model I predicts a more strongly decaying transient current and slower discharging. Features of the early calculations on transient space-charge-limited current, such as a peak in the external current when charges reach the counterelectrode,[22] are reproduced for model II.

For both models, though a fit to the experimental behavior could be obtained in the charging period, discharging was in general too slow. In this respect, we would like to stress the necessity to unravel the nature of charging and discharging currents: in the models, we have considered that current originates only from transport of injected carriers. Dipolar contributions have not been dealt with because polyethylene is normally a weakly polar material, and hence this contribution is expected to be low. However, low frequency dielectric spectroscopy data are not easily available in the literature to support this hypothesis and to state up to which current level this is actually so. In the same way, low mobility ionic species could contribute to the external current. This normally should give rise to heterocharge formation. However, the limited resolution of space charge measurement techniques close to the interface, possibly combined with injection (formation of homocharges), may prevent evidence of such processes being obtained from PEA data. Hence, attempting to explain space charge accumulation and transient currents by a single process may be misleading.

[1]T. Tanaka, T. Okamoto, K. Nakanishi, and T. Miyamoto, IEEE Trans. Electr. Insul. **28**, 826 (1993).
[2]T. Takada, IEEE Trans. Dielectr. Electr. Insul. **6**, 519 (1999).
[3]T. Mizutani, IEEE Trans. Dielectr. Electr. Insul. **1**, 923 (1994).
[4]J. C. Fothergill, L. A. Dissado, J. Alison, and A. See, Proceedings of the Conference on Dielectric Materials, Measurements and Applications, Edinburgh, UK, 17–21 September 2000 (IEEE, Piscataway, New Jersey, 2000), pp. 352–356.
[5]T. Maeno, IEEE Trans. Dielectr. Electr. Insul. **8**, 845 (2001).
[6]K. Fukunaga, IEEE Electr. Insul. Mag. (USA) **20**, 18 (2004).
[7]R. J. Fleming, M. Henriksen, and J. T. Holbøll, IEEE Trans. Dielectr. Electr. Insul. **7**, 561 (2000).
[8]G. M. Sessler, IEEE Trans. Dielectr. Electr. Insul. **4**, 614 (1997).
[9]G. Teyssedre, C. Laurent, G. C. Montanari, F. Palmieri, A. See, L. A. Dissado, and J. C. Fothergill, J. Phys. D **34**, 2830 (2001).
[10]G. Teyssedre, C. Laurent, A. Aslanides, N. Quirke, L. A. Dissado, G. C. Montanari, A. Campus, and L. Martinotto, IEEE Trans. Dielectr. Electr. Insul. **8**, 744 (2001).
[11]Y. Tanaka, G. Chen, A. Vaughan, and T. Takada, Proceedings of the International Conference on Properties and Applications of Dielectric Materials, Nagoya, Japan, 1–5 June 2003 (IEEE, Piscataway, New Jersey, 2003), pp. 970–973.
[12]S. Le Roy, P. Segur, G. Teyssedre, and C. Laurent, J. Phys. D **37**, 298 (2004).
[13]F. Boufayed, S. Le Roy, G. Teyssedre, C. Laurent, P. Segur, E. Cooper, L. A. Dissado, and G. C. Montanari, Proceedings of the International Conference on Solid Dielectrics, Toulouse, France, 5–9 July 2004 (IEEE, Piscataway, New Jersey, 2004), pp. 562–566.
[14]J. M. Alison and R. M. Hill, J. Phys. D **27**, 1291 (1994).
[15]K. Kaneko, T. Mizutani, and Y. Suzuoki, IEEE Trans. Dielectr. Electr. Insul. **6**, 152 (1999).
[16]M. Fukuma, M. Nagao, and M. Kosaki, Proceedings of the International Conference on Properties and Applications of Dielectric Materials, Brisbane, Australia, 3–8 July 1994 (IEEE, Piscataway, New Jersey, 1994), pp. 24–27.
[17]S. Le Roy, G. Teyssedre, P. Segur, and C. Laurent, Proceedings of the International Conference on Electrical Insulation and Dielectric Phenomena, Boulder, Colorado, 17–20 October 2004 (IEEE, Piscataway, New Jersey, 2004), pp. 29–32.
[18]S. Le Roy, G. Teyssedre, G. C. Montanari, F. Palmieri, and C. Laurent, J. Phys. D **39**, 1427 (2006).
[19]M. Meunier, N. Quirke, and A. Aslanides, Proceedings of the International Conference on Electrical Insulation and Dielectric Phenomena, Victoria, BC, 17–20 October 2000 (IEEE, Piscataway, New Jersey, 2000), pp. 21–24.
[20]J. C. Fothergill and L. A. Dissado, *Space Charge in Solid Dielectrics* (The Dielectrics Society, Leicester, UK, 1998).
[21]N. F. Mott and E. A. Davis, *Electronic Processes in Non-Crystalline Materials*, 2nd ed. (Clarendon, Oxford, 1979).
[22]A. Rose, Phys. Rev. **97**, 1538 (1955).
[23]G. C. Montanari and P. H. F. Morshuis, IEEE Trans. Dielectr. Electr. Insul. **12**, 754 (2005).
[24]M. Meunier, A. Aslanides, and N. Quirke, J. Chem. Phys. **115**, 2876 (2001).
[25]J. A. Anta, G. Marcelli, M. Meunier, and N. Quirke, J. Appl. Phys. **92**, 1002 (2002).
[26]S. Le Roy, G. Teyssedre, and C. Laurent, IEEE Trans. Dielectr. Electr. Insul. **13**, 239 (2006).
[27]P. K. Banerjee, *The Boundary Element Methods in Engineering*, 2nd ed. (McGraw-Hill, Paris, 1994).
[28]B. P. Leonard, Comput. Methods Appl. Mech. Eng. **88**, 17 (1991).
[29]W. H. Press, B. P. Flannery, S. A. Teukolsky, and W. T. Vetterling, *Numerical Recipes* (Cambridge University Press, Cambridge, 1986), Chap. 17.
[30]S. Le Roy, G. Teyssedre, and C. Laurent, IEEE Trans. Dielectr. Electr. Insul. **12**, 644 (2005).
[31]F. Boufayed, S. Le Roy, G. Teyssedre, C. Laurent, P. Segur, E. Cooper, L. A. Dissado, and G. C. Montanari, Proceedings of the 2004 Conference of "Société Française d'Electrostatique," Poitiers, France, 2–3 September 2004 (Société Française d'Electrostatique, Futuroscope, France, 2004), pp. 474–478.
[32]A. Many and G. Rakavy, Phys. Rev. **126**, 1980 (1962).
[33]S. Le Roy, G. Teyssedre, P. Segur, and C. Laurent, Proceedings of the International Conference on Properties and Application of Dielectric Materials, Nagoya, Japan, 1–5 June 2003 (IEEE, Piscataway, New Jersey, 2003), pp. 859–862.
[34]J. M. Alison, Meas. Sci. Technol. **9**, 1737 (1998).
[35]Y. Suzuoki, H. Kon, K. Kaneko, T. Mizutani, and T. Itaya, *Space Charge in Solid Dielectrics* (The Dielectrics Society, Leicester, UK, 1998), pp. 303–309.